Scripta Materialia 138 (2017) 32–34

Contents lists available at ScienceDirect

Scripta Materialia

journal homepage: www.elsevier.com/locate/scriptamat

Regular Article

Evaluating boron-carbide constituents with simulated Raman spectra

Cody Kunka, Amnaya Awasthi, Ghatu Subhash *

University of Florida, Gainesville, FL 32611, USA

ARTICLE INFO

Article history:
Received 2 May 2017
Received in revised form 18 May 2017
Accepted 19 May 2017
Available online 25 May 2017

Keywords:
Boron carbide
Raman spectroscopy
Polymorphism
Density functional theory

ABSTRACT

Boron carbide exhibits extraordinary mechanical, thermal, and chemical properties but also has a complex structure due to extensive polymorphism. In particular, each fabricated sample of boron carbide likely comprises a collection of crystal structures mixed at the nanoscale. Development of methods to quantify these polymorphic variants would facilitate understanding and tailoring of properties. Hence, the current investigation provides a methodology to approximate the distribution of Raman-active constituents through comparison of an experimental Raman scan with a superposition of simulated Raman spectra. For boron carbide, the results indicate that hot pressing yields a different distribution of crystal structures than spark-plasma sintering.

Ceramics often exhibit a high propensity for variation in their crystal structures (e.g., polymorphs, polytypes, allotropes, isomorphs, and isomers). For example, silicon carbide has over 250 polytypes [1], and boron carbide is speculated to have hundreds of polymorphs [2]. Identification of these structural variants typically comprises quantum-mechanical calculations of Gibbs free energy (i.e., the sum of static/lattice, internal, phonon, and pressure-volume energies [3]). Because this calculation requires significant computational expense, many studies exclusively report static energy [4]. However, this approximation forgoes kinetics considerations (e.g., temperature-dependent polymorphic transformations [5]) and may incorrectly predict fabricated structures [6]. Unfortunately, even including all contributors to Gibbs free energy does not guarantee correct prediction for systems that have energetically similar structural variants [7]. For those cases, researchers often rely on a comparison of experimental and theoretical properties (e.g., TEM diffraction and spectroscopies). For decades, comparison methodology has been employed to analyze the structure of boron carbide [2]. However, success has been greatly limited by the large number of proposed polymorphs and by the tendency for fabricated samples to contain several crystal structures mixed at the nanoscale (i.e., below experimental resolution) [8]. Hence, this manuscript approximates components of both hot-pressed and spark-plasma-sintered boron carbide by fitting experimental Raman scans with simulated Raman spectra.

Raman scans of both hot-pressed (HP) and spark-plasma-sintered (SPS) boron carbide are performed with 532-nm wavelength, 250-mW energy, 1800-l/mm grating, 1-s exposure, and 1-μm spatial resolution. This green wavelength is the most common for measuring the Raman spectra of boron carbide [2]. Also, each scan (i.e., HP and SPS) can be considered representative of its processing method because the experimental Raman spectrum of boron carbide was shown to be independent of stoichiometry [9]. Next, these two experimental Raman scans are normalized and deconvoluted with the Renishaw WiRE® 4.3 software [see "EXP" curves in Fig. 1]. These deconvolutions recreate the experimental spectra within 0.01% error. Note that the locations (i.e., wavenumbers) of the dominant Raman peaks are nearly identical for HP and SPS samples. These shared, dominant peaks are labeled "A" through "K" in Fig. 1. The major differences between these two spectra are only the relative intensities of several peaks (especially 266, 320, 480, 533, and 825 cm^{-1}).

To evaluate the fabricated constituents, Raman spectra are simulated to match the aforementioned deconvoluted peaks. For this study, stoichiometry of simulated polymorphs is limited to B_4C (i.e., 20 at.% C), which offers high theoretical stability [10–14], Raman activity [15], and consistency between experimental and simulated twinning behaviors [16]. Also, α-rhombohedral boron (i.e., α-B_{12}) is included because prior studies speculated that this crystal structure may be formed in boron carbide [10,17]. To offer comprehensive and efficient simulation of boron-carbide polymorphs, this investigation employs the recently modified nomenclature: *zijk* [18]. Here, *z* specifies the site number(s) of icosahedral carbon(s), and *ijk* specifies chain permutation. For example, this nomenclature can differentiate 3,5BCB [i.e., ($B_{10}C_{p3,p5}$)BCB] from 1,4BCB [i.e., ($B_{10}C_{p1,p4}$)BCB], but the traditional nomenclature considers both to be ($B_{10}C_{2p,antipodal}$)BCB. Hence, by using this revised nomenclature, all B_4C unit cells that have twelve-atom icosahedra and three-atom linear chains can be modeled.

Ground-state electronic configurations and static energies are calculated with density functional theory (DFT) in ABINIT [19] with periodic unit cells, 4 × 4 × 4 Monkhorst *k*-point meshes, 30-Ha (816-eV) cutoff energy, Troullier-Martins norm-conserving pseudopotentials, and the

* Corresponding author.
E-mail address: subhash@ufl.edu (G. Subhash).

http://dx.doi.org/10.1016/j.scriptamat.2017.05.030
1359-6462/

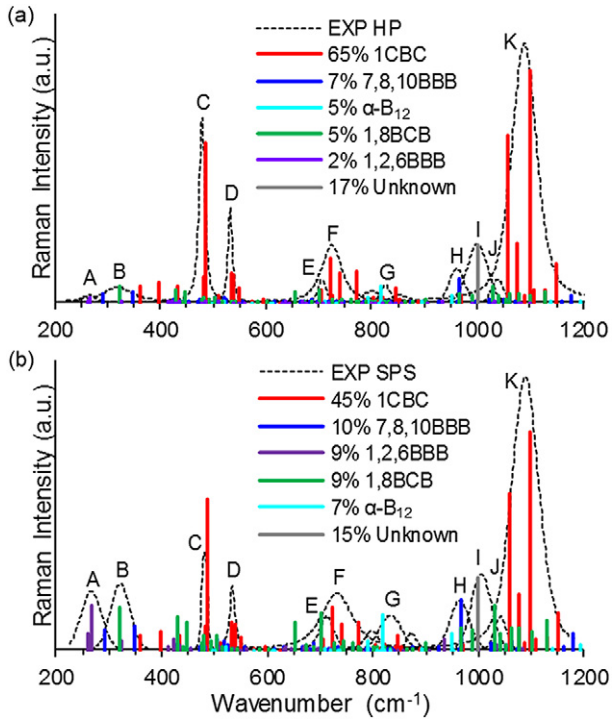

Fig. 1. Fitting of deconvoluted experimental Raman spectra (dotted curves) with quantum mechanical simulations. Differences between (a) HP and (b) SPS boron carbide seem to be merely relative abundances.

Teter-Pade local-density approximation (LDA) [20]. We chose this exchange-correlation functional over the generalized-gradient approximation (GGA) because of a prior experimental comparison [18]. As validation, we have also reproduced the static energies of six boron-carbide polymorphs reported in another study [21] within 0.5% error. After relaxation, elastic tensors and natural frequencies are calculated with density functional perturbation theory (DFPT) [22] under the harmonic approximation. Except for 1,2,3BBB and 1,2,9BBB, all fifty-nine unique B_4C structures (i.e., "equivalent-lattice groups" [18]) are found to be both elastically stable (i.e., having positive values for all four elastic-stability criteria [23]) and dynamically stable (i.e., lacking negative natural frequencies). Table 1 ranks all stable crystal structures by their static energies (E_{static}), which are listed relative that of 1CBC, the most abundant polymorph [2].

For the stable crystal structures, Raman intensities are calculated with the post-processing deployed by the WURM project [24,25]. This method is independent of crystallographic orientation and explicitly incorporates both excitation frequency (i.e., 532 nm) and temperature (i.e., 300 K). As a validation of the Raman-simulation parameters, we have reproduced peak positions of multiple Raman spectra in the WURM database [24] and of both experimental and simulated Raman spectra of α-B_{12} [26,27] within 0.5% error. For conciseness, Table 1 reports the top three dominant peaks for each structure (plus the next six for 1CBC). Peaks within 11 cm^{-1} of a deconvoluted experimental (EXP) peak are labeled with superscripts corresponding to the peak locations of Fig. 1 (i.e., "A" through "K"). This buffer should account for deviation due to the harmonic approximation [28] and ensures that the most abundant polymorph (i.e., 1CBC) matches the most dominant experimental peaks.

An experimental Raman spectrum represents the combination of characteristic scattering events from all constituents in the interaction volume, and the relative contribution of each constituent is directly proportional to its relative abundance. Hence, the relative abundance of a constituent is determined by the scaling factor required for fitting that constituent's simulated spectrum to a dominant peak in the experimental spectrum. The harmonic approximation and pseudopotentials only induce small errors, so simulated polymorphs with strong dominant Raman peaks in regions far from experimental peaks (e.g., 1160 cm^{-1} of 0CCC) are disqualified as constituents. As suggested by experimental peak splitting [26], nearby peaks can superimpose if peak separation

Table 1
Static energies (E_{static}) and dominant Raman peaks for all stable B_4C polymorphs and for α-boron. B_4C static energies are relative 1CBC. Superscripts indicate agreement of simulated wavenumbers with the twelve experimental (EXP) peaks shown in Fig. 1.

Structure	E_{static}	Dominant Raman peaks			Structure	E_{static}	Dominant Raman peaks		
zijk	*meV*	*EXP Peak*(cm^{-1}; *a.u.*)			*zijk*	*meV*	*EXP Peak*(cm^{-1}; *a.u.*)		
1CBC	0	^{K}(1099; 1.00)	(1058; 0.72)	^{C}(486; 0.69)	1,5BCB*	304	(975; 1.00)	(1015; 0.76)	(454; 0.62)
		(1076; 0.25)	^{F}(724; 0.19)	(1151; 0.17)	1,7BCB	305	(214; 1.00)	(1053; 0.44)	^{C}(470; 0.42)
		(772; 0.13)	^{D}(534; 0.12)	(740; 0.12)	7,11BCB	314	(345; 1.00)	(453; 0.68)	(672; 0.67)
7CBC	35	^{K}(1082; 1.00)	(1118; 0.60)	(512; 0.50)	1,11BCB	316	(281; 1.00)	^{D}(363; 0.42)	(1625; 0.40)
0CCC	77	(1160; 1.00)	(758; 0.87)	^{K}(1098; 0.53)	1,2BCB	328	^{A}(264; 1.00)	^{A}(264; 1.00)	(348; 0.96)
7,8BBC	151	^{J}(1045; 1.00)	^{J}(1036; 0.95)	(1120; 0.64)	7,8,9BBB	337	^{B}(325; 1.00)	^{H}(966; 0.13)	(853; 0.08)
1,10CBB	156	(1068; 1.00)	(492; 0.92)	^{J}(1031; 0.75)	1,4BCB	346	^{H}(968; 1.00)	(502; 0.77)	(453; 0.70)
7BCC	166	(1067; 1.00)	^{F}(724; 0.52)	(355; 0.38)	1,7,10BBB	352	(424; 1.00)	^{A}(263; 0.61)	(974; 0.54)
4BCC	169	(1062; 1.00)	(1160; 1.00)	(377; 0.79)	1,2,4BBB	356	^{A}(268; 1.00)	(304; 0.65)	(393; 0.46)
1BCC	174	(354; 1.00)	(1071; 0.89)	(1685; 0.46)	7,8,10BBB	358	^{H}(966; 1.00)	(348; 0.49)	(291; 0.40)
1,8BBC	176	(1056; 1.00)	^{C}(477; 0.81)	(1113; 0.64)	1,8,9BBB	359	(296; 1.00)	(981; 0.16)	^{D}(522; 0.10)
1,7BBC	193	(307; 1.00)	^{C}(471; 0.69)	(439; 0.50)	1,5,8BBB	373	(932; 1.00)	(452; 0.93)	(462; 0.87)
7,10BBC	199	(1019; 1.00)	(1061; 0.65)	^{D}(535; 0.58)	1,10,11BBB	375	(350; 1.00)	(293; 0.68)	(985; 0.27)
1,11CBB	201	(347; 1.00)	(431; 0.74)	^{J}(1033; 0.63)	1,8,10BBB	375	(379; 1.00)	(977; 0.91)	^{A}(258; 0.79)
1,5BBC	202	(344; 1.00)	(1074; 0.88)	(1024; 0.65)	1,8,11BBB	379	(331; 1.00)	(975; 0.66)	(1164; 0.56)
1,2BBC	221	(341; 1.00)	(1019; 0.56)	(378; 0.35)	1,7,8BBB	384	(379; 1.00)	(415; 0.43)	^{I}(1000; 0.43)
10BCC	225	(394; 1.00)	(1668; 0.58)	(1140; 0.45)	7,8,12BBB	405	(337; 1.00)	(988; 0.64)	(415; 0.47)
1,2CBB	229	^{B}(324; 1.00)	(362; 0.99)	(420; 0.43)	1,5,9BBB	414	^{A}(267; 1.00)	^{B}(315; 0.94)	(1021; 0.24)
1,10BBC	228	(334; 1.00)	(461; 0.71)	^{J}(1046; 0.37)	1,11,12BBB	415	^{B}(319; 1.00)	^{B}(324; 0.20)	(978; 0.13)
1,8CBB	232	(360; 1.00)	^{K}(1100; 0.68)	^{J}(1043; 0.64)	1,8,12BBB	423	(351; 1.00)	(304; 0.75)	^{I}(992; 0.65)
7,11BBC	246	^{J}(1036; 1.00)	(1167; 0.50)	(510; 0.49)	1,2,10BBB	430	^{A}(265; 1.00)	(398; 0.42)	^{B}(327; 0.35)
1,4BBC	248	^{B}(309; 1.00)	(457; 0.93)	^{J}(1034; 0.84)	1,2,7BBB	432	(378; 1.00)	^{A}(266; 0.49)	(459; 0.27)
1,7CBB	260	(404; 1.00)	(455; 0.70)	(1074; 0.66)	1,7,11BBB	433	(250; 1.00)	(307; 0.90)	(362; 0.33)
7,10BCB	265	(1063; 1.00)	(689; 0.68)	^{F}(723; 0.68)	1,4,7BBB	440	(394; 1.00)	(580; 0.41)	(212; 0.40)
1,11BBC	271	(352; 1.00)	(307; 0.24)	^{J}(1040; 0.17)	1,2,12BBB	442	(245; 1.00)	(351; 0.80)	(429; 0.48)
1,10BCB	272	^{A}(257; 1.00)	(1059; 0.41)	(678; 0.28)	1,2,6BBB	442	^{A}(266; 1.00)	^{A}(262; 0.39)	(934; 0.25)
7,8CBB	283	(364; 1.00)	(412; 0.66)	^{J}(1050; 0.50)	1,5,7BBB	443	(404; 1.00)	^{A}(254; 0.63)	(373; 0.61)
7,8BCB	287	(347; 1.00)	(1604; 0.56)	(417; 0.32)	1,4,8BBB	455	(300; 1.00)	^{A}(263; 0.63)	(226; 0.31)
1,8BCB	289	^{J}(1029;1.00)	^{B}(322; 0.98)	^{E}(702; 0.83)	α-B_{12}	–	^{G}(818; 1.00)	^{H}(951; 0.46)	(791; 0.24)

and widths are appropriate. For example, the simulated peaks of 1CBC at 1059 cm^{-1} and 1099 cm^{-1} likely superimpose to form experimental peak K (1089 cm^{-1}). The high scaling factor required for fitting this peak translates to 65 at.% for HP boron carbide and 45 at.% for SPS boron carbide [see Fig. 1] and is consistent with prior work [2]. Also, 1CBC can account for peaks C (479 cm^{-1}), D (532 cm^{-1}), and F (725 cm^{-1}). We attribute peak G (825 cm^{-1}) to α-B_{12} and note that no structure with B_4C stoichiometry could account for this peak. This selection of α-B_{12} is consistent with the fact that boron clusters are sometimes considered minority constituents [8,27] and proposed to form during solid-state amorphization [29–32]. Peaks A (265 cm^{-1}), B (319 cm^{-1}), and H (961 cm^{-1}) can be attributed to polymorphs with multiple icosahedral carbons (e.g., 7,8,10BBB, 1,8BCB, and 1,2,6BBB). Many of these structures were previously overlooked.

To establish the origin of peak I (998 cm^{-1}), future simulations of other boron phases [17,33], defected/twinned structures [16,34], non-B_4C stoichiometries (e.g., polymorphs without Raman-activity [2] and/or with two/four-atom chains [14,35–37]), or heterogeneous supercells [38] are recommended. To identify non-Raman-active constituents, other spectroscopies would prove useful. To more easily distinguish crystal structures that produce similar Raman peaks and to determine when an experimental peak is a superposition of nearby peaks, peak widths could be included with anharmonic simulations [28]. To include the interactions of dissimilar constituents, supercells could be simulated if computational expense decreases. However, although these potential improvements would further generalize our method, the current form still provides a powerful prediction.

This investigation has presented a novel and efficient method for predicting relative abundances of constituents in complex materials through comparison of experimental and quantum-mechanically simulated spectra. This method has been applied to quantify the constituents produced in hot-pressed and spark-plasma-sintered boron carbide. Based on the similarities of the dominant Raman-active natural frequencies, it was argued that these two processing methods yield the same crystal structures but at different abundances. The identification of the majority constituent (i.e., 1CBC) was consistent with multiple prior investigations, and several minority constituents have been identified for the first time. In particular, the association of the relative abundance of α-B_{12} with the Raman peak near 825 cm^{-1} could be particularly helpful for understanding the amorphization of boron carbide [32].

Acknowledgements

This work is supported by the Army Research Office under Grant No. ARO-W911NF-14-1-0230 and by the National Science Foundation under Grants DGE-1315138 (Graduate Reserch Fellowship Program) and ACI-1053575 (Extreme Science and Engineering Discovery Environment TG-MSS15006). The ABINIT code is a common project of the Université Catholique de Louvain, Corning Inc., the Université de Liège, the Commissariat à l'Energie Atomique, Mitsubishi Chemical Corp., the Ecole Polytechnique Palaiseau, and other contributors (*http://www.abinit.org*).

References

[1] R. Cheung, Silicon Carbide Microelectromechanical Systems for Harsh Environments, Imperial College Press, 2006.
[2] V. Domnich, S. Reynaud, R. Haber, M. Chhowalla, J. Am. Ceram. Soc. 94 (2011) 3605.
[3] L. Zhong-Li, Comput. Phys. Commun. 191 (2015) 150.
[4] A. Gavezzotti, G. Filippini, J. Am. Chem. Soc. 117 (1995) 12299.
[5] B.P. Van Eijck, W.T.M. Mooij, J. Kroon, J. Comput. Chem. 22 (2001) 805.
[6] J. Nyman, G.M. Day, CrystEngComm 17 (2015) 5154.
[7] C. Hammond, The Basics of Crystallography and Diffraction, Oxford University Press, 2001 28.
[8] G. Fanchini, J. McCauley, M. Chhowalla, Phys. Rev. Lett. 97 (2006).
[9] D.R. Tallant, T.L. Aselage, A.N. Campbell, D. Emin, Phys. Rev. B Condens. Matter 40 (1989) 5649.
[10] N. Vast, J. Sjakste, E. Betranhandy, 16th International Symposium on Boron, Borides and Related Materials, 7–12 Sept. 2008, IOP Publishing Ltd, UK, 2009 012002 (18 pp.).
[11] D. Taylor, J. McCauley, T. Wright, J. Phys. Condens. Matter 24 (2012).
[12] S. Konovalikhin, V. Ponomarev, J. Phys. Chem. 84 (2010) 1445.
[13] D. Wang, Q. Yan, B. Wang, Y. Wang, J. Yang, G. Yang, J. Chem. Phys. 140 (2014).
[14] A. Ektarawong, S.I. Simak, L. Hultman, J. Birch, F. TasnÃ¡di, F. Wang, B. Alling, J. Chem. Phys. 144 (2016).
[15] A.N. Enyashin, A.L. Ivanovskii, Phys. Solid State 53 (2011) 1569.
[16] K.Y. Xie, Q. An, M.F. Toksoy, J.W. McCauley, R.A. Haber, W.A. Goddard, K.J. Hemker, Phys. Rev. Lett. 115 (2015) 175501.
[17] B. Albert, H. Hillebrecht, Angew. Chem. Int. Ed. 48 (2009) 8640.
[18] C. Kunka, A. Awasthi, G. Subhash, Scr. Mater. 122 (2016) 82.
[19] X. Gonze, B. Amadon, P. Anglade, J. Beuken, F. Bottin, P. Boulanger, F. Bruneval, D. Caliste, R. Caracas, M. Cote, et al., Comput. Phys. Commun. 180 (2009) 2582.
[20] S. Goedecker, M. Teter, J. Hutter, Phys. Rev. B 54 (1996) 1703.
[21] S. Aydin, M. Simsek, Phys. Status Solidi B 246 (2009) 62.
[22] X. Gonze, M. Verstraete, C. Audouze, M. Torrent, F. Jollet, International Conference of Computational Methods in Sciences and Engineering 2009: (ICCMSE 2009), 29 Sept.–4 Oct. 2009, American Institute of Physics, USA, 2012 944.
[23] J. Wang, Z. Wang, Y. Jing, S. Wang, C. Chou, H. Hu, S. Chiou, C. Tsoo, W. Su, Solid State Commun. 244 (2016) 12.
[24] R. Caracas, E. Bobocioiu, Am. Mineral. 96 (2011) 437–443.
[25] R. Caracas, E. Bobocioiu, Theoretical Modelling of Raman Spectra, EMU, 2011.
[26] I. Chuvashova, E. Bykova, M. Bykov, V. Svitlyk, B. Gasharova, Y. Mathis, R. Caracas, L. Dubrovinsky, N. Dubrovinskaia, J. Solid State Chem. 245 (2017) 50.
[27] H. Werheit, V. Filipov, U. Kuhlmann, U. Schwarz, M. Armbruster, A. Leithe-Jasper, T. Tanaka, I. Higashi, T. Lundstrom, V.N. Gurin, et al., Sci. Technol. Adv. Mater. 11 (2010).
[28] R. Caracas, E.J. Banigan, Phys. Earth Planet. Inter. 174 (2009) 113.
[29] X. Yan, W. Li, T. Goto, M. Chen, Appl. Phys. Lett. 88 (2006).
[30] D. Ghosh, G. Subhash, H.L. Chee, K.Y. Yoke, Appl. Phys. Lett. 91 (2007), 061910.
[31] S. Aryal, P. Rulis, W.Y. Ching, Phys. Rev. B 84 (2011) 184112 (12 pp.).
[32] G. Subhash, A. Awasthi, C. Kunka, P. Jannotti, M. DeVries, Scr. Mater. 123 (2016) 158.
[33] Q. An, K.M. Reddy, K.Y. Xie, K.J. Hemker, W.A. Goddard, Phys. Rev. Lett. 117 (2016), 085501.
[34] Q. An, W.A. Goddard, K.Y. Xie, G. Sim, K.J. Hemker, T. Munhollon, M.F. Toksoy, R.A. Haber, Nano Lett. (2016).
[35] K. Shirai, K. Sakuma, N. Uemura, Phys. Rev. B 90 (2014) 064109 (10 pp.).
[36] G. Kwei, B. Morosin, J. Phys. Chem. 100 (1996) 8031.
[37] A. Ektarawong, S. Simak, B. Alling, Phys. Rev. B 94 (2016), 054104.
[38] G.P. Harikrishnan, K.M. Ajith, C. Sharat, M.C. Valsakumar, Evolutionary algorithm based structure search and first-principles study of B12C3 polytypes, J. Alloys Compd. 695 (0925-8388) (2017) 2023–2034, http://dx.doi.org/10.1016/j.jallcom.2016.11.040.